Design of a Multivariable Flutter Suppression/Gust Load Alleviation System

B. S. Liebst,* W. L. Garrard,† and Jerome A. Farm‡
University of Minnesota, Minneapolis, Minnesota

This paper discusses the use of eigenspace techniques for the design of an active flutter suppression/gust load alleviation system for a hypothetical research drone. One leading-edge and two trailing-edge aerodynamic control surfaces and four sensors (accelerometers) are available for each wing. Full-state control laws are designed by selecting feedback gains which place closed-loop eigenvalues and shape closed-loop eigenvectors so as to stabilize wing flutter and reduce gust loads at the wing root while yielding acceptable robustness and satisfying constraints on rms control surface activity. These controllers are realized by state estimators designed using an eigenvalue placement/eigenvector shaping technique which results in recovery of the full-state loop transfer characteristics. The resulting feedback compensators are shown to perform almost as well as the full state designs. They also exhibit acceptable performance in situations in which the failure of an actuator is simulated.

Nomenclature

Vectors

c_i	= ith row of measurement matrix
u	= control input
v_i	= attainable closed-loop eigenvector associated with λ_i eigenvalue
v_i^d	= desired closed-loop eigenvector associated with λ_i eigenvalue
w_i	= vector used in calculation of gain matrix
x	= system state
$\hat{x}$	= estimate of system state
y	= measurement vector (accelerometer outputs)
Γ	= disturbance input vector
ξ_s	= vector of flexural generalized coordinates
ξ_c	= control surface displacement vector
μ_i	= the left zero-direction of the ith finite transmission zero

Matrices

A_m	= aerodynamic coefficient matrix
A	= open-loop dynamics matrix
B	= control distribution matrix
C	= measurement matrix
C_s	= structural damping matrix
$G(s)$	= open-loop transfer matrix, $C(sI\text{-}A)^{-1}B$
$F(s)$	= full-state loop transfer matrix, $K(sI\text{-}A)^{-1}B$
$H(s)$	= compensator transfer matrix, $K(sI\text{-}A\text{-}BK+LC)^{-1}L$
$H(s)G(s)$	= loop transfer matrix
K	= control gain matrix
L	= estimator gain matrix
K_s	= structural stiffness matrix
M_s	= structural mass matrix
P_i	= eigenvector weighting matrix associated with ith eigenvector
$Q_c(s)$	= calculated unsteady aerodynamic influence coefficient matrix
$Q_A(s)$	= s-plane approximation of unsteady aerodynamic influence coefficient matrix
S	= nonsingular square matrix of order m
V	= matrix whose columns are v_i
W	= matrix whose columns are w_i

Scalars

c	= reference chord, 14 in. Also local chord in Fig. 1.
j	= $\sqrt{-1}$
J_i	= ith performance index
L	= reference length in Dryden gust model, 1700 ft
M	= Mach number
m	= number of controls
n	= number of states
$\bar{q}$	= dynamic pressure
q	= fictitious noise weighting term
s	= Laplace operator
V	= forward velocity
z_i	= ith transmission zero
β	= aerodynamic lag reduced frequency, $\omega c/2V = 0.13$
η	= zero mean white noise input to gust model, intensity $(L/V)\xi_g^2$
λ_i	= ith eigenvalue
ω	= circular frequency
ξ_g	= vertical wind gust velocity
ξ_g	= rms vertical wind gust velocity
ϕ_i	= influence coefficient associated with ith flexure mode

Superscripts

d	= desired
$*$	= complex transpose
T	= transpose
-1	= inverse

Received July 15, 1986; presented as Paper 86-2247 at the AIAA Guidance, Navigation and Control Conference, Williamsburg, VA, Aug. 18-20, 1986; revision received May 8, 1987.

*Assistant Professor, Department of Aerospace Engineering and Mechanics; currently with Contraves-Goerz, Pittsburgh, PA. Senior Member AIAA.

†Professor, Department of Aerospace Engineering and Mechanics. Associate Fellow AIAA.

‡Graduate Research Assistant, Department of Aerospace Engineering and Mechanics; currently with McDonnell-Douglas, St. Louis, MO.

Introduction

METHODS for the design of systems for active control of aerodynamic wing flutter have been proposed by numerous authors.[1-10] Classical single-input-single-output

(SISO) techniques,[1,2] the aerodynamic energy method,[2] linear quadratic regulator (LQR) theory,[3-9] and eigenspace techniques[9,10] have been applied to design of flutter control systems. All of the design techniques listed above, except classical SISO procedures, are easily applied to the design of multivariable controllers; however, most studies of flutter control systems have concentrated on the use of a single control surface per wing. Since failure of the flutter control system could result in catastrophic failure of the wing, two or more control surfaces per wing might result in improved safety. Also, improved performance might result.

In this paper, eigenspace techniques are used to design a flutter control system for a mathematical model of the wing of a hypothetical flight test vehicle. The model of the wing structure and aerodynamics is of an actual research drone vehicle with a high aspect ratio, supercritical wing designed to flutter within the flight envelope.[1-10] This drone has only a single control surface per wing for flutter control; for the current study, additional surfaces are added to the mathematical model so that true multi-input-multi-output (MIMO) control system designs can be studied. Models with two and three control surfaces per wing are used. Both leading- and trailing-edge surfaces are considered.

It is shown that eigenspace design techniques which allow direct placement of closed-loop eigenvalues and shaping of closed-loop eigenvectors[11] can be used to design full-state controllers which stabilize the wing, reduce wing root gust loads, and result in good multivariable stability margins without exceeding constraints on rms control surface deflections and rates. These full-state controllers are then realized by the use of dynamic state estimators. An eigenspace procedure which is very similar to the regulator design technique is used to design state estimators which exhibit loop transfer properties similar to the full-state designs. The resulting compensators, which convert accelerometer outputs to actuator inputs, are shown to perform adequately even when the failure of a control surface is simulated.

Performance Requirements and Mathematical Models

The planform of the wing to be controlled is shown in Fig. 1. The leading-edge (LE) and two trailing-edge (TE) control surfaces and the four accelerometer locations are indicated. The control-surface locations were selected to provide good control effectiveness for the aeroelastic modes. Sensor locations were selected to be as nearly collocated with control surfaces as physical constraints would allow. Various combinations of these surfaces and accelerometers are examined. The design flight condition is at a Mach number of 0.86 and an altitude of 15,000 ft (this corresponds to a velocity of 909 fps and a dynamic pressure of 4.29 psi). At this flight condition, the flutter control system is required to stabilize the wing without exceeding rms control surface displacements of 15 deg and displacement rates of 740 deg/s under a 12 fps rms vertical wind gust.

The aeroelastic model of the wing is given as

$$([M_s]s^2+[C_s]s+[K_s])[\xi_s]+\bar{q}[Q_c(s)]\begin{bmatrix}\xi_s\\ \xi_c\\ \xi_g\end{bmatrix}=0 \tag{1}$$

$[Q_c(s)]$ is calculated as a function of reduced frequency by a doublet lattice procedure and is approximated by the matix of transfer functions

$$[Q_A(s)]=[A_0]+[A_1][cs/2V]+[A_2][cs/2V]^2+[A_3]s/(s+(2V/c)\beta) \tag{2}$$

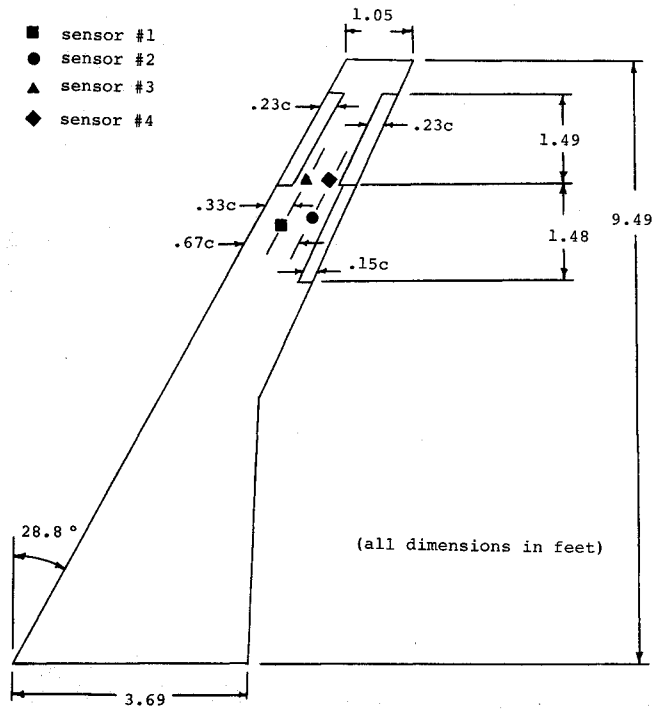

Fig. 1 Planform of wing.

where β and the elements of the matrices A_i, $i=0...3$, are selected to give the best least-squares fit to Q_c over the range of reduced frequencies for which Q_c is calculated. This type of model has been widely used to represent unsteady aerodynamic forces in the design of flutter control systems.[1-10]

This study uses a model comprised of five flexure modes to represent the aeroelastic behavior of the wing. In this model, mode 1 is essentially pure bending, modes 2 and 3 are combined bending and torsion, mode 4 is essentially pure torsion and mode 5 is primarily bending. The natural frequencies of these modes at zero dynamic pressure are 45.15 rad/s, 185.51 rad/s, 197.51 rad/s, 325.93 rad/s, and 434.14 rad/s, respectively. A structural damping factor of 0.005 is assumed for each mode. The locus of the open-loop aeroelastic roots of the wing with varying velocity is shown in Fig. 2. This locus of roots was generated by neglecting the variation of Q_c with Mach number. As velocity increases, the damping in the first elastic root initially increases but then decreases and the wing flutters at a velocity of 896 fps. This model does not contain longitudinal rigid body modes. In a previous study,[10] it was found that the frequencies associated with the aeroelastic response of the wing were so much higher than those of the rigid body modes that the aeroelastic response of the wing and the rigid body response were uncoupled. Thus in gust-load alleviation, the elevator is effective only in reducing the lowest frequency component of the wing root loads and the wing-tip ailerons used for flutter suppression were only useful in reducing the high-frequency components of these loads. Design of control systems for reduction of high- and low-frequency components of the gust loads can be performed independently.

The control surface actuator transfer functions are identical and are

$$\xi_{ci}(s)/u_i(s)=1.7744728\times10^7/(s+180)\times[s^2+251s+(314)^2] \tag{3}$$

The vertical wind gust is modeled by a second-order Dryden model

$$\xi_g(s)/\eta(s)=[1+(\sqrt{3}L/V)s]/[1+(L/V)s]^2 \tag{4}$$

The rms gust velocity is 12 fps.

Equations (1–4) can be combined to give the mathematical model for the wing, control surfaces and actuators, and wind gust in vector matrix form as

$$\dot{x} = Ax + Bu + \Gamma\eta \tag{5}$$

The order of this model is 26. The state vector for the wing consists of five structural displacements, five corresponding rates, five unsteady aerodynamic states, nine control states (three for each surface), and two gust states. The motion of the wings can be sensed by up to four accelerometers mounted on the front and rear spars of each wing (see Fig. 1). The output of each accelerometer can be expressed as

$$\begin{aligned} y_i &= \Sigma\phi_i\ddot{\xi}_{si} = f_i\dot{x} \\ &= f_i(Ax + Bu + \Gamma\eta) \\ &= f_iAx + f_iBu + f_i\Gamma\eta \end{aligned} \tag{6}$$

However, $f_iB = 0$, and $f_i\Gamma\eta$ is negligible, therefore,

$$y_i = f_iAx = c_ix \tag{7}$$

Thus, the measurement vector is

$$y = Cx \tag{8}$$

Theory of Eigenspace Design

A common method for the design of multivarible control systems is to use LQR theory to design full-state controllers which achieve desired performance and to realize these controllers via Kalman filters which provide estimates of the system states.[12] For full-state LQR controllers, the minimum singular value of the return difference matrix is always greater than or equal to one. This guarantees gain margins of at least ± 6 db with no variations in phase, and phase margins of ± 60 deg with no variations in gain.[13] These stability margins are not necessarily retained if a Kalman filter is used in the feedback loop to estimate the system state.[14] However, stability margins of the full-state controller can be recovered if the Kalman filter is designed using the loop transfer recovery (LTR) method of Doyle and Stein.[14] This technique has been used in several studies of active flutter suppression systems.[4,5,8]

In this paper, eigenspace techniques are used to design both full-state control laws and estimators which result in compensators with loop transfer properties which approximate those of the full-state controller. Eigenspace design techniques for full-state feedback control laws select feedback gains which place closed-loop eigenvalues in desired positions and which, if there is more than one control, shape closed loop eigenvectors. Some basic results for eigenspace design are briefly summarized below. More detailed discussions can be found in Refs. 9–11 and 15.

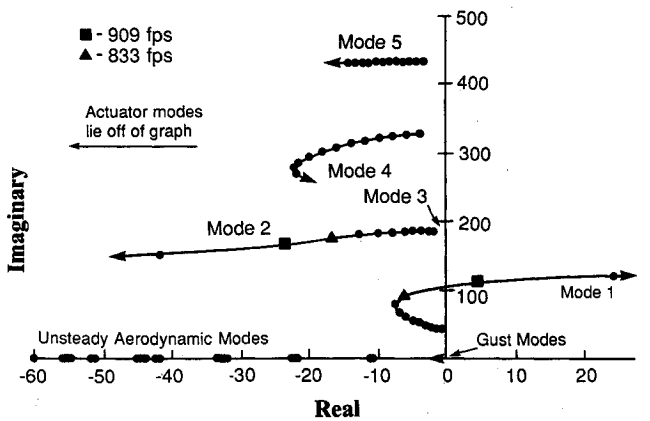

Fig. 2 Locus of open loop aeroelastic roots with velocity.

Eigenspace Regulator Design

Consider a system described by Eq. (5) with a linear control law

$$u = Kx \tag{9}$$

where $\mathrm{Dim}(x) = n$ and $\mathrm{Dim}(u) = m$. If the system is controllable and B is full rank, the following results can be proven.[11,15]

1) The position of n closed-loop eigenvalues can be arbitrarily assigned.

2) A total of m elements of each eigenvector can be arbitrarily selected subject to the constraint that the eigenvector associated with the eigenvalue λ_i must lie in the subspace spanned by $(I\lambda_i - A)^{-1}B$.

If it is desired to move an eigenvalue, the design procedure consists of determining the gain matrix K such that for all desired closed-loop eigenvalue and eigenvector pairs (λ_i, v_i),

$$(A + BK)v_i = \lambda_i v_i \tag{10}$$

This is equivalent to finding an m-dimensional vector w_i such that

$$(I\lambda_i - A)v_i = Bw_i \tag{11}$$

Once the w_i's have been found, the gain matrix is calculated as

$$K = W[V]^{-1} \tag{12}$$

Since the desired eigenvectors are, in general, not achievable, the w_i's are selected to minimize the weighted least-squares difference between the elements of the desired and the attainable eigenvectors, as given by the following performance index:

$$J_i = (v_i - v_i^d)^* P_i (v_i - v_i^d) \tag{13}$$

where P_i is a positive definite symmetric matrix whose elements can be chosen to weight the difference between certain elements of the desired and attainable eigenvectors more heavily than others. The procedure for solving the above problem is given in Ref. 10.

Eigenspace Estimator Design

Once the full-state regulator gains, K, have been determined, the problem of constructing a state estimate, $\hat{x}$, from measurements, y, must be addressed. A common estimation/control scheme is as follows:

$$u = K\hat{x}$$

where

$$\dot{\hat{x}} = A\hat{x} + Bu + L(y - C\hat{x})$$

The task is to choose estimator gains, L, such that $A - LC$ is stable, and the performance (as measured by various methods, e.g., transfer functions, rms response, stability robustness, etc.) of the regulator/estimator closely resembles that for full-state feedback. For MIMO systems the stability robustness is typically measured by the smallest minimum singular value for the return difference matrix occurring in a bounded frequency range. A value near one for this minimum singular value indicates good stability robustness.[14]

In the full-state feedback case the return difference matrix is

$$I - F(s)$$

and in the combined regulator/estimator case it is

$$I-H(s)G(s)$$

In the SISO case it is clear that if one wishes to recover $F(s)$ then L should be chosen such that

$$H(s)\approx F(s)/G(s)$$

inverting the plant by sending the poles of $H(s)$ to the zeroes of $G(s)$. Care must be taken to assure that the eigenvalues of the estimator, $A-LC$, are stable.

A technique for designing L in the MIMO case to recover $F(s)$ was proposed by Doyle and Stein.[14] They showed that LTR of full-state regulators can be achieved with a Kalman estimator by adding fictitious noise q^2BB^T directly to the input of the plant during the estimator design. For $q=0$ the ordinary Kalman estimator results. As q is increased the LTR improves, resulting in the recovery of full-state stability robustness. A key result from Ref. 14 is that as $q\to\infty$ the estimator gains $L\to qBS\to\infty$, and the estimator poles asymptotically approach the finite transmission zeroes of $G(s)$ (i.e., plant inversion) and infinity. The finite transmission zeroes of $G(s)$ can be determined from

$$\det\begin{bmatrix} z_iI-A & B \\ -C & 0 \end{bmatrix}=0$$

A recent paper by Kazerooni and Houpt[16] explains how LTR can be achieved with a completely different approach based upon eigenspace placement. As shown in Ref. 14, if L is chosen such that

$$\frac{L(q)}{q}\to BS \text{ as } q\to\infty \tag{14}$$

then $H(s)$ approaches pointwise (i.e., nonuniformly)

$$K(sI-A)^{-1}B[C(sI-A)^{-1}B]^{-1}$$

and therefore

$$H(s)G(s)\to F(s) \tag{15}$$

Thus, by picking

$$L=qBS \tag{16}$$

Equation (14) will be satisfied and the LTR of Eq. (15) will be achieved as $q\to\infty$. Reference 16 shows that, for a minimum phase plant, as $q\to\infty$ the consequences of choosing L as in Eq. (16) are:

1) The $j\le n-m$ finite closed-loop eigenvalues, λ_i, of $A-LC$ and $A+BK-LC$ approach the finite transmission zeroes, z_i, of the plant.

2) The remaining $n-j$ closed-loop eigenvalues approach infinite at any angle.

3) The left closed-loop eigenvector v_i of $A-LC$ associated with the finite closed-loop estimator eigenvalue, λ_i, approaches the left zero-direction, μ_i, of the transmission zero, z_i, which satisfies

$$[\mu_i^T\zeta_i^T]\begin{bmatrix} z_iI-A & B \\ -C & 0 \end{bmatrix}=0 \tag{17}$$

4) $H(s)G(s)\to F(s)$ pointwise.

The finite asymptotic eigenstructures resulting from both Eq. (14) and Eq. (16) are the same, but the asymptotic infinite eigenstructures are generally different. If S is selected arbitrarily, the form of L given by Eq. (16) may not result in a stable estimator. Since both forms guarantee the pointwise approach of $H(s)G(s)$ to $F(s)$, we would expect any estimator with the finite asymptotic structure of 1-3 to achieve LTR. Therefore, for a minimum phase system, an estimator which combines any stable infinite eigenstructure with the finite eigenstructure of 1-3 would result in LTR.

The procedure for the design of estimators which achieve LTR with the eigenspace placement algorithms previously described is as follows:

1) Determine the finite transmission zeroes, z_i, and associated left zero-directions, μ_i, from Eq. (17).

2) Drive j finite eigenvalues of $A-LC$ to (or near) the finite transmission zeroes, z_i. The associated desired (and in this case, attainable) left eigenvectors should be chosen as μ_i.

3) Place the remaining $n-j$ eigenvalues of $A-LC$ at locations far into the left-half plane. The desired left eigenvectors for these modes are chosen arbitrarily and have little effect on the LTR.

4) As with the Doyle-Stein procedure, improved LTR is obtained as the finite eigenvalues are moved closer to the transmission zeroes and as the infinite eigenvalues are moved further left. Therefore, several iterations may be required before sufficient recovery is achieved.

Difficulties in using this LTR procedure will arise if the plant has right-half plane transmission zeroes (nonminimum phase). Placing the estimator poles at these right-half plane

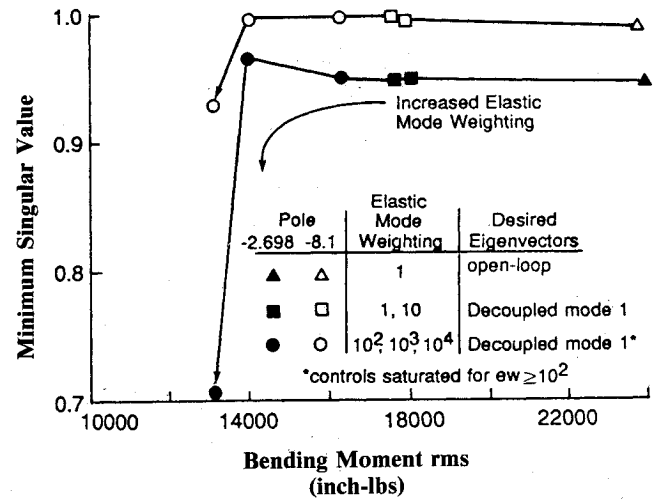

Fig. 3 Effect of elastic mode weighting on eigenvalue placement on bending moment and minimum singular value.

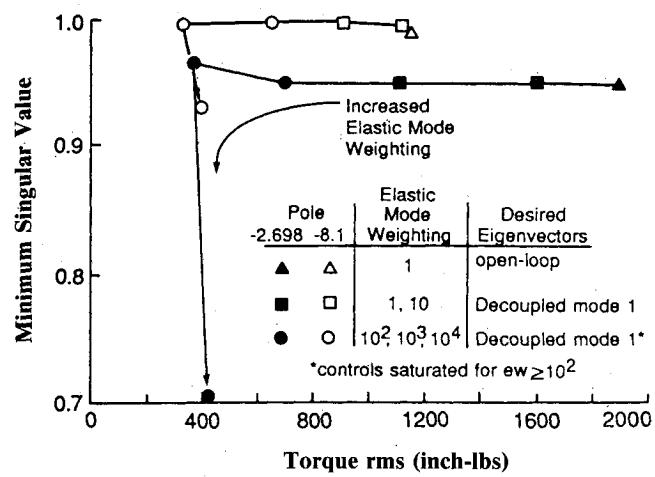

Fig. 4 Effect of elastic mode weighting and eigenvalue placement on torque and minimum singular value.

zeroes would result in an unstable system. The Doyle-Stein procedure in the case of a nonminimum phase plant selects the stable Riccati solution for the estimator which drives the poles to the mirror image of any unstable transmission zeroes. Thus, a stable estimator is obtained but LTR is not guaranteed. If there are no right-half plane transmission zeroes in the frequency range over which LTR is important, then placement of estimator poles at the mirror image of right-half plane transmission zeroes typically achieves reasonable LTR.

Full State Feedback Design

The design process is as follows: First, closed-loop eigenvalue locations are selected to obtain the best stability robustness results achievable without excessive control surface activity. Once a suitable eigenvalue configuration has been established, the associated closed-loop eigenvectors are selected to reduce wing root loads as much as possible without compromising stability margins or causing control surface saturation. Eigenvector shaping is used explicitly for both gust-load reduction and balancing activity among the control surfaces. After a full-state controller has been designed, a compensator that converts accelerometer outputs to control inputs is designed, using an eigenspace technique that results in recovery of the loop transfer properties of the full-state control laws.

In the discussion which follows, unless otherwise stated, all results are for a control system using all three control surfaces. In the design of the flutter suppression/gust load alleviation system, all of the stable open-loop eigenvalues are used as desired closed-loop eigenvalues. However, at the design velocity the aircraft is unstable, having unstable eigenvalues at $+2.698 \pm j109.9$. Two closed-loop positions for these poles are considered. The first position is obtained simply by "flipping" the unstable eigenvalues into the left-half plane to $-2.698 \pm j109.9$. This is the placement that would result from LQR theory if minimum control energy were specified.[12] This placement has yielded good results in previous designs.[9,10] The second position, $-8.1 \pm j109.9$, is obtained by moving the poles twice as far to the left as they were moved when they were flipped about the imaginary axis. In both cases the open-loop eigenvectors are used as the initial choices for desired eigenvectors. It can be seen in Figs. 3 and 4 that the $-8.1 \pm j109.9$ placement yields higher minimum singular values, and, hence, a more robust system than the $-2.698 \pm j109.9$ location. This is not surprising as the damping ratio has been increased. In addition, comparing Tables 1 and 2 reveals that this placement does not cost significantly more in terms of control effort. Comparing the triangular points in Figs. 3 and 4 reveals that incremental bending moment is unaffected while incremental torque is actually reduced by using this eigenvalue placement. Moving the real part of this eigenvalue still further to the left results in increased control surface activity.

With the closed-loop eigenvalues positioned, the choices for closed-loop eigenvectors are then optimized. Since the first bending mode (mode 1) is the principal contributor to wing root bending moment, the energy in this mode is reduced by setting to zero the elements in the desired mode 1 eigenvector which correspond to all other structural modes. In all other desired eigenvectors, elements corresponding to the displacement and rate of mode 1 are set equal to zero. This results in a 25% reduction in bending moment. A smaller reduction is achieved in torque since the first bending mode has a small torque component.

By altering P_i in Eq. (13) to increase the weightings on the elastic-mode elements of the eigenvectors, the elements of the elastic mode eigenvectors are made to approach the desired values more closely. This improves the bending mode decoupling described above, and reduces bending moment and torque as depicted in Figs. 3 and 4. The minimum singular value remains relatively constant as elastic mode weightings are increased up to a weighting of 10^3, then decreases rapidly, and robustness suffers for higher elastic mode weightings. The price of reduced gust loads is increased rms displacment of the LE surface. Elastic mode weightings of 100 or greater produce control saturation of the LE surface (Tables 1 and 2).

Since only the LE surface saturates, and the workload is not evenly distributed between the control surfaces, the control weightings are altered to force a more even distribution of the workload between the surfaces. By increasing the weightings for eigenvector components corresponding to the LE surface, those components are reduced. As a result, the LE surface

Table 1 Effects of increasing elastic mode weightings on rms control surface activity (mode 1 pole: $-2.698 \pm j109.9$)

	Elastic mode weightings				
	1	10	100	1000	10,000
Surface			Deflection (deg)		
TE Outboard	3.077	7.359	14.69	12.6	11.21
TE Inboard	9.425	3.836	0.8752	1.91	3.956
LE	3.873	11.83	20.28[a]	24.22[a]	23.74[a]
Surface			Rate (deg/sec)		
TE Outboard	47.36	95.43	168.7	142.4	124.1
TE Inboard	117.2	51.95	9.2	25.7	50.42
LE	59.63	137.5	229.6	277.2	275.4

[a]Saturated

Table 2 Effects of increasing elastic mode weightings on rms control surface activity (mode 1 pole: $-8.1 \pm j109.9$)

	Elastic mode weightings				
	1	10	100	1000	10,000
Surface			Deflection (deg)		
TE Outboard	3.074	7.368	14.7	12.6	11.21
TE Inboard	9.438	3.845	0.878	1.912	3.958
LE	3.890	11.84	20.28[a]	24.22[a]	23.74[a]
Surface			Rate (deg/sec)		
TE Outboard	49.69	97.44	167.9	141.4	123.2
TE Inboard	123.7	56.21	10.94	25.62	50.3
LE	66.18	139.7	229.2	276.5	275.0

[a]Saturated

works less, while the others work more. Equalization of control surface activity is done for elastic-mode weightings of 100, 1000, and 10,000. By evenly distributing the workload, saturation of the LE surfaces is avoided, and it is possible to increase elastic-mode weightings to 10,000. This results in a reduction of 50% in bending moment, compared to a 25% reduction possible without distributing the workload.

In Fig. 5, it can be seen that the bending moment depends largely on the elastic-mode weightings and is relatively insensitive to the control-mode weightings. Since all of the control surfaces are near the tip of the wing, they have nearly the same moment arm and are all roughly as effective in reducing bending moment. It can also be seen that torque depends greatly on control-mode weightings. As LE control mode weightings are increased and the control surface workload is more evenly distributed, a torque unbalance is created between the two trailing-edge surfaces and the single leading-edge surface and therefore torque increases. Thus, even distribution of the workload between the three surfaces allows elastic-mode weightings to be increased to reduce bending moment at the expense of increased torque. In Tables 1 and 2 it can be seen that the trailing-edge inboard surface does not work very hard for higher elastic-mode weightings. Since the TE inboard surface is smaller and has a smaller moment arm than the TE outboard surface, it is not quite so effective as the other surfaces in reducing bending moment, and the controller does not use it very much.

Since the control effort of the TE inboard surface is low, and since making it work more causes a torque imbalance, a two-control system without the TE inboard surface is examined as well. Removing this surface from the system reduces the order of the system to 23. This system exhibits higher bending moment and lower torque than the three-control case due to the lack of the TE inboard surface. The two-control case has higher minimum singular values as well. This illustrates the conservative nature of utilizing the minimum singular value of the return difference matrix as a stability robustness measure.

Based on the trade-offs outlined above, closed-loop eigenvalue/eigenvector placements for the full-state design are selected as follows. All eigenvalues except the unstable pair are placed in their open-loop positions. Since these eigenvalues do not cause difficulties, it was not necessary to use control efforts to move them. The unstable pair is placed at $-8.1 \pm j109.9$ and the desired eigenvectors are decoupled as described above. Two eigenvector weighting schemes are chosen, one each for the three- and two-control cases. Both designs use eigenvector shaping to balance control effort. This allows the use of elastic mode weightings of 10,000 in the three-control surface case. This results in the lowest bending moments of any of the designs, torques which compared favorably to other weighting schemes, and a good minimum singular value. For the two-control case, elastic-mode weightings of 100 are used. The main features of this design are high minimum singular value and low torque. Control mode weightings are given in Table 3. It is found that

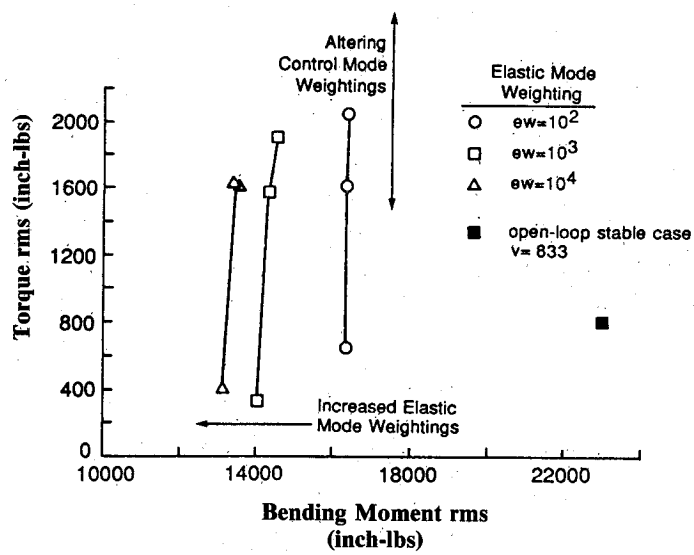

Fig. 5 Effect of elastic mode weighting and control mode weighting on torque and bending moment.

Table 3 Final full-state feedback designs

	3-control	2-control	Open-loop	3-control	2-control
Velocity (fps)	909	909	833	833	833
			Weightings		
			Elastic modes		
	10,000	100	–	10,000	100
			Control surfaces		
TEO (x,v,a)[a]	60,1,1	90,1,1	–	60,1,1	90,1,1
TEI (x,v,a)	110,1,1	1,1,1	–	110,1,1	1,1,1
LE (x,v,a)	120,1,1	60,1,1	–	120,1,1	60,1,1
			RMS responses		
			Control deflections (deg)		
TE Outboard	11.97	10.09	0.	11.77	9.92
TE Inboard	10.49	–	0.	10.82	–
LE	11.91	8.878	0.	11.92	8.71
			Control rates (deg/s)		
TE Outboard	135.0	129.6	0.	125.1	113.4
TE Inboard	126.3	–	0.	121.1	–
LE	139.7	114.7	0.	130.4	101.0
Bending moment (in.-lb)	14600	20550	22980	12000	20550
Shear (lb)	440.0	474.8	412.1	382.8	474.8
Torque (in.-lb)	1945	1048	817.5	1574	1048
Minimum singular value	0.929	0.996	–	0.904	0.972

[a] x = dispacement, v = rate, a = acceleration

weightings on control surface rate and acceleration must be kept low compared with weightings on the displacement or robustness suffers. The performance of the two systems at a velocity at which the system is open-loop stable (833 fps) is also shown in Table 3. It can be seen that for the three-control case, a significant decrease in bending moment is obtained, shear is about the same and torque is doubled. Since the bending moment is an order of magnitude greater than the torque, a significant reduction in total wing root load is achieved.

Loop Transfer Recovery

With the full-state feedback regulator gains K designed, the state estimator gains L are determined using the previously described LTR method. This method requires a square system. Four sensors (accelerometers) are available as shown in Fig. 1. The sensors closest to the control surfaces are the ones chosen as this results in the most robust design. Thus, the three-control system uses sensors 2, 3, and 4, and the two-control system uses sensors 3 and 4.

Figure 6 shows the estimator poles and the finite open-loop transmission zeroes for the three-control case. Six of the calculated transmission zeroes are very small. These six zeroes come from the double differentiations resulting from each accelerometer and should be exactly on the origin. (The limitations of finite precision arithmetic are responsible for three zeroes not lying exactly on the origin.) In order to keep the magnitude of the estimator gains as small as possible, the open-loop estimator poles are assigned to the closest transmission zeroes. The $L=0$ estimator eigenvalues corresponding to plant poles 3 and 5, gust poles, and unsteady aerodynamic poles are sent to nearby transmission zeroes. The $L=0$ estimator eigenvalues associated with the actuator poles are sent to infinity. The remaining six eigenvalues are sent to six transmission zeroes at the origin.

The six estimator poles which should, in the limit, approach the origin are termed "zero" poles. The effects of moving these zero poles toward the origin can be seen in Figs. 7 and 8. The zero pole scaling represents the approximate magnitude of the zero poles. A zero pole scaling of one places the zero poles of the estimator at a distance of one from the origin, as this

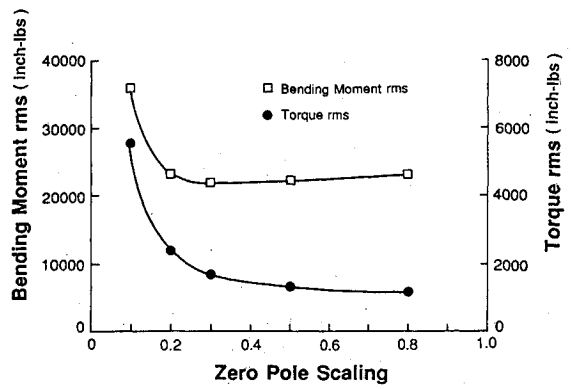

Fig. 8 Effect of finite estimator pole location on bending moment and torque.

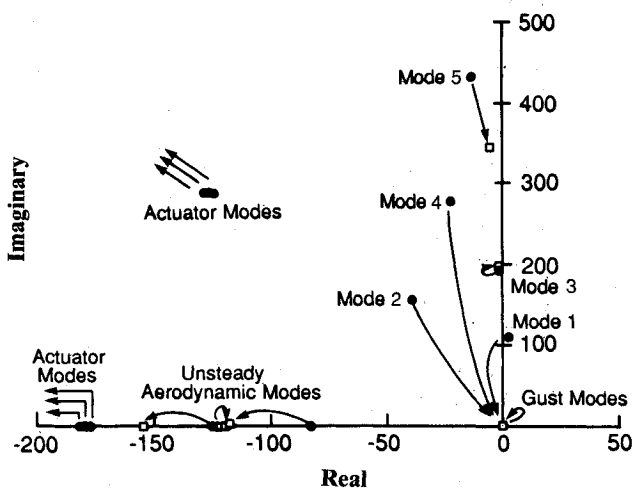

Fig. 6 Estimator Poles and open-loop transmission zeros for three-control case (estimator poles, transmission zeros).

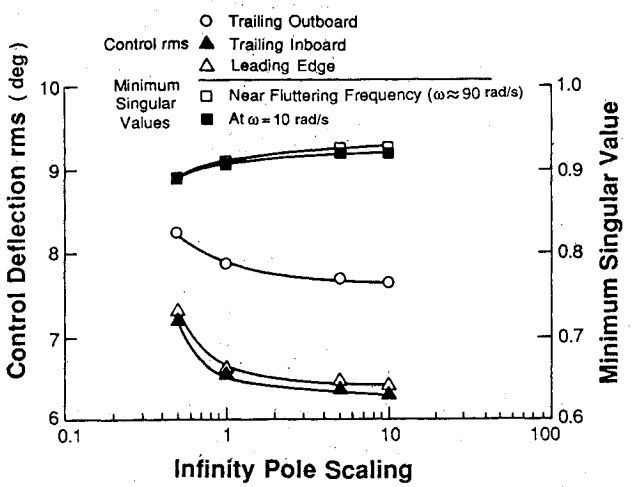

Fig. 9 Effect of infinite estimator pole location on minimum singular value and control surface deflection.

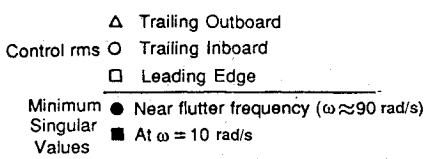

Fig. 7 Effect of finite estimator pole location on minimum singular value and control surface deflection.

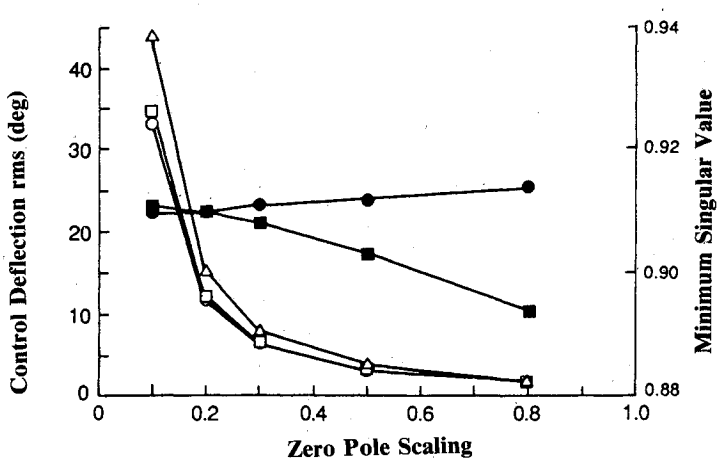

scaling goes to zero, the zero poles approach the origin. Decreasing the zero pole scaling increases bending moment, torque and control deflections. It can be seen that for a zero pole scaling less than 0.3, these quantities increase rapidly. As shown in Fig. 9, the minimum singular value achieves minima at frequencies of approximately 10 and 90 rad/s. Decreasing the zero pole scaling slightly decreases the minimum singular value at 90 rad/s and increases the minimum singular value at 10 rad/s. A zero pole scaling of 0.3 was chosen to obtain good minimum singular values without control saturation and excessive wing root loads.

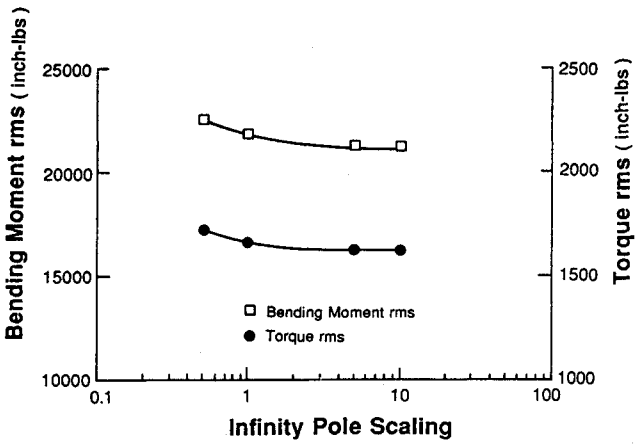

Fig. 10 Effect of infinite estimator pole location on bending moment and torque.

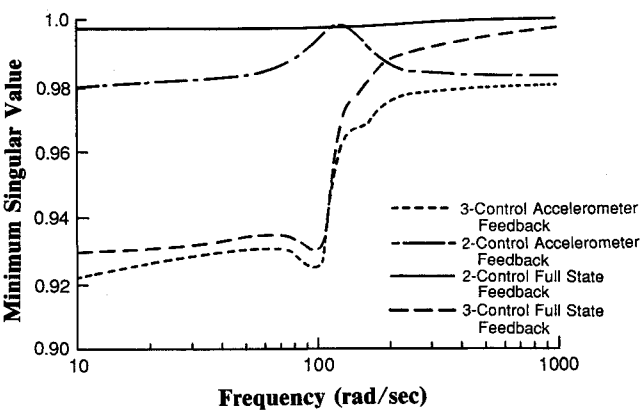

Fig. 11 Minimum singular values of the return difference matrices vs frequency.

After selecting a zero pole scaling, the large magnitude estimator poles ("infinity" poles) were similarly scaled. An estimator infinity pole with scaling of one is defined as a pole with a magnitude of 880, a value well above the magnitudes of the finite estimator poles. Increasing the magnitude of the infinity poles reduces bending moment, torque, and control rms (Figs. 10 and 11), while increasing the minimum singular value. The zero pole scaling for these figures is also 0.3 as chosen above. Moving the infinity poles toward infinity also greatly increases the estimator feedback gains. An infinity pole scaling of five is chosen, since larger scalings do not significantly improve performance or robustness. This results in infinity poles of magnitude 4400 rad/s. This is about ten times the size of the largest poles in the aeroelastic wing model. If these high-frequency poles cause implementation problems, they can be eliminated by residualization of the estimator.[4] As can be seen from Figs. 10 and 11, the locations of the finite estimator poles have a much greater effect on both the rms responses and the singular values than do the locations of the infinite estimator poles. With the Doyle-Stein approach to LTR all estimator poles move simultaneously, and, thus, it is not possible to evaluate the effects of independently varying the locations of the finite and infinite estimator poles.[14]

Final Designs

The results for the final regulator/estimator designs are summarized in Table 4 and Figs. 12, 13. Compared with the full-state designs in Table 3, it can be seen that, other than for bending moment in the three-control case, the performance parameters (control activity, wing root structural loads, and minimum singular values) have been nearly recovered. Figure 9 shows clearly the loop transfer recovery by plotting the minimum singular values of the return difference matrices vs frequency for both of the systems with full-state feedback and with estimators in the feedback loops. It can be seen that even at high frequencies good LTR is achieved. Figure 12, the closed-loop root locus for the three-control case shows that flutter suppression is achieved. The closed-loop onset of flutter is at a velocity of 941 fps. This corresponds to a 5% increase in flutter velocity compared with the open-loop case. The two-control closed-loop root locus is not shown but is very similar to Fig. 12.

In a previous study[10] a 28% increase in flutter speed was achieved using a different mathematical model of the wing. In an attempt to increase the flutter speed of the wing modeled in this study, the real parts of the poles associated with the

Table 4 Performance of final compensator designs

Velocity (fps)	3-control 909	2-control 909	Open-loop 833	3-control 833	2-control 833
			RMS control deflection (deg)		
TE Outboard	7.669	8.231	–	7.374	7.873
TE Inboard	6.366	–	–	6.092	–
LE	6.469	6.333	–	6.19	6.054
			RMS control rate (deg/s)		
TE Outboard	65.93	90.78	–	42.37	50.67
TE Inboard	55.98	–	–	33.48	–
LE	57.51	73.95	–	33.58	40.93
Bending moment (in.-lb)	21310	22090	22980	19430	20640
Shear (lb)	464.3	466.2	412.1	420.1	428.0
Torque (in.-lb)	1632	1286	817.5	1141	813.3
Minimum singular value	0.922	0.979	–	0.91	0.977
MIMO Gain margin (db) $20 \log [1/(1 \pm MSV)]$[a]	22, −5.7	33.6, −5.9	–	22, −5.7	38.4, −6
MIMO phase margin (deg) $\pm \cos^{-1} [1-(MSV^2)/2]$	±54.9	±58.6	–	±54.9	±59.2

[a]MSV = Minimum singular value

unstable mode were moved further to the left. The results are shown in Table 5. In order to achieve a 17% increase in flutter speed, the real parts of these poles had to be moved to −200 rad/s. With full-state feedback, the control surface activity was within acceptable bounds, but with the compensator in the loop, control surface deflections exceeded the allowable limits. It is felt that the inability to achieve a larger increase in flutter speed is due to changing the wing model without changing the design point. In this study, the specified design condition was at a speed of 909 fps, and the flutter speed was 896 fps. In the previous example,[10] the design speed was also 909 fps, but the flutter speed was 750 fps. Thus, the design speed was considerably greater than the flutter speed in the previous study while, in this study, the flutter and design speeds were very close. It should be noted that the closed-loop flutter speed in the previous study was 960 fps compared to 941 fps for this study, a difference of only 2%. If a greater percentage increase in flutter speed is desired, the design speed should be selected to be higher.

Table 6 shows the performance of the control systems at an open-loop stable flight condition. This table illustrates the bending moment gust-load alleviation achieved with the controllers. Notice that the two-control case achieves bending moment reduction with no increase in torque. The three-control case achieves even greater bending moment reductions but at the expense of an increase in torque.

Minimum singular values for the two- and three-control cases are plotted vs velocity in Fig. 13. The minimum singular values peak at the design velocity, hence the systems are most robust at this velocity. Above the design velocity the system rapidly loses robustness, becoming unstable near 941 fps (4.53 psi). The addition of the compensator to the system has, as desired, raised the velocity at which the wing becomes unstable. At lower velocities the singular value is somewhat reduced but never falls below 0.9 for the two-control case and 0.8 for the three-control case. Thus, the flutter control system does not cause the wing to be unstable at velocities where it is open-loop stable.

The effects of various control surface failures were examined by setting the column corresponding to the failed control to zero in the control gain matrix K. This represents a control failure which is undetected. In Table 6, it can be seen that

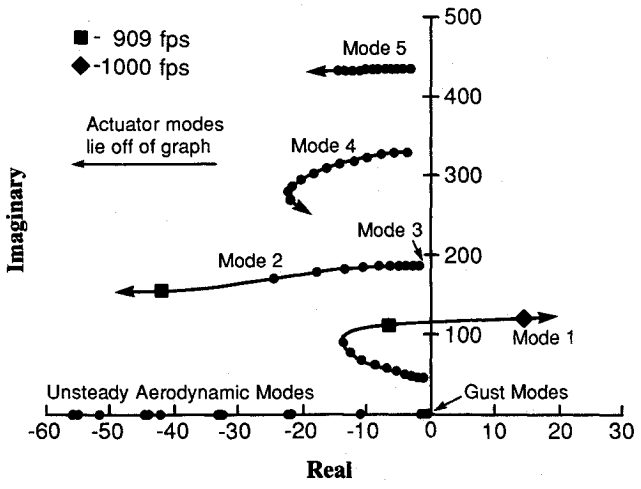

Fig. 12 Locus of closed loop elastic roots with velocity.

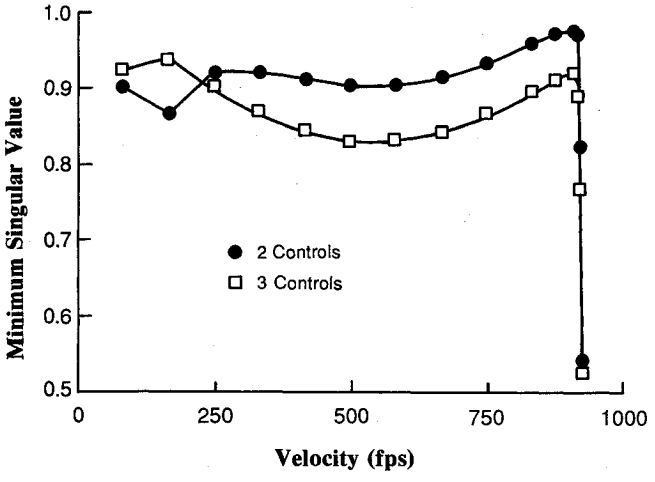

Fig. 13 Minimum singular values of the return difference matrices vs velocity.

Table 5 Effects of mode 1 pole placement

Mode 1 pole position (real part)	−8.1[a]	−40[a]	−80[a]	−200[a]	−40[b]	−200[b]
			RMS control responses (deg)			
			Control deflection (deg)			
TE Outboard	12.09	12.1	12.1	12.1	18.6[c]	24.1[c]
TE Inboard	10.44	10.46	10.47	10.48	22.48[c]	60.43[b]
LE	11.77	11.78	11.77	11.76	17.65[c]	29.9[c]
			Control rates (deg/s)			
TE Outboard	136.2	135.8	137.4	150.7	134.8	305.5
TE Inboard	125.7	130.8	137.4	151.5	87.44	159.0
LE	138.4	137.8	133.8	138.9	94.29	253.8
			RMS structural responses[a]			
Minimum singular value	0.93	0.947	0.962	0.952	0.915	0.9
Flutter velocity (fps)	941	987	1011	1052	[c]	[c]
Flutter velocity increase (%)	5	10	13	17	[c]	[c]

(Full-state responses were constant to within a few percent.)

Bending Moment (in-lb)	14660
Shear (lb)	446
Torque (in.-lb)	1962

[a]Full-state regulator, [b]Regulator/estimator, [c]Control saturation

Table 6 Effects of a single control failure on final compensator designs

	3-control			2-control	
Failed control:	TEO	TEI	LE	TEO	LE
	RMS control deflection (deg)				
TE Outboard	–	8.218	8.059	–	8.406
TE Inboard	5.968	–	6.157	–	–
LE	6.199	6.38	–	6.374	–
	RMS control rate (deg/s)				
TE Outboard	–	82.72	81.6	–	131.
TE Inboard	82.43	–	72.14	–	–
LE	83.41	73.93	–	173.9	–
	Minimum singular value				
	0.527	0.644	0.679	0.293	0.583
	MIMO gain margin (db) $20 \log[1/(\pm \text{MSV})]$[a]				
	6.5, −3.7	9.0, −4.3	9.9, −4.0	3.0, −2.2	7.6, −4.0
	MIMO phase margin (deg) $\pm \cos^{-1}[1-(\text{MSV}^2)/2]$				
	±30.6	±37.6	±39.6	±16.8	±33.9

[a]MSV = Minimum singular value

the loss of a control surface reduces the minimum singular value and increases control surface rms. However, none of the designs becomes unstable and no control surfaces saturate for any failure mode. Using the results of Ref. 17, guaranteed MIMO gain margins (with no change in phase) and MIMO phase margins (with no change in gain) are given. It can be seen that even in the worse case, failure of the trailing-edge outboard surface in the two-control case, gain margins of +3.0 and −2.2 DB and phase margins of ±16.8 deg are maintained.

Conclusions

Eigenspace techniques have been applied to the design of an active flutter suppression/gust load alleviation system for a hypothetical model of a wing with leading- and trailing-edge control surfaces. Both the regulator and estimator designs were obtained using eigenspace placement algorithms. Robust flutter stabilization was achieved by eigenvalue placement, and wing root loads were reduced by eigenvector shaping. The full-state regulator properties were then recovered by direct placement of estimator eigenvalues and eigenvectors at or near the plant transmission zeroes and associated left zero-directions. An important conclusion is that control effort should be balanced between the leading and trailing edge to provide bending moment reduction without an increase in torque.

Acknowledgments

The research reported in this paper was partially supported by NASA Langley Research Center under Grant NAG-1-217 with Mr. William M. Adams as technical monitor, by NSF Grant DMS-8413129, and by a grant from the Academic Computer Center of the University of Minnesota.

References

[1]Abel, I., Newsom, J.R., and Dunn, H.J., "Application of Two Synthesis Techniques for Active Flutter Suppression of an Aeroelastic Wind Tunnel Model," AIAA Paper 79-1633, Aug. 1979.

[2]Schmidt, D.K. and Chen, T.K., "Frequency Domain Synthesis of a Robust Flutter Suppression Control Law," *Journal of Guidance, Control, and Dynamics,* Vol. 9, May-June 1986, pp. 346-351.

[3]Newsom, J.R., "Control Law Synthesis Using Optimal Control Theory," *Journal of Guidance and Control,* Vol. 2, Sept.-Oct. 1979, pp. 388-394.

[4]Mahesh, J.K., Stone, C.R., Garrard, W.L., and Dunn, H.J., "Control Law Synthesis for Flutter Suppression Using Linear Quadratic Control Theory," *Journal of Guidance and Control,* Vol. 4, July-Aug. 1981, pp. 382-395.

[5]Garrard, W.L., Mahesh, J.K., Stone, C.R., and Dunn, H.J., "Robust Kalman Filter Design for Active Flutter Suppression," *Journal of Guidance, Control and Dynamics,* Vol. 5, July-Aug. 1982, pp. 412-414.

[6]Takahashi, M. and Slater, G.L., "Design of a Flutter Mode Controller Using Positive Real Feedback," *Journal of Guidance, Control and Dynamics,* Vol. 9, May-June 1986, pp. 399-345.

[7]Newsom, J.R., "Design of the Flutter Suppression System for a Remotely Piloted Research Vehicle (DAST ARW-1R)," AIAA Paper 83-0990, May 1983.

[8]Adams, W.M. and Tiffany S.H., "Design of a Candidate Flutter Suppression Law for the DAST ARW-2," NASA TM 86257, July 1984.

[9]Garrard, W.L. and Liebst, B.S., "Active Flutter Suppression Using Eigenspace and Linear Quadratic Design Techniques," *Journal of Guidance, Control and Dynamics,* Vol. 8, May-June 1985, pp. 304-311.

[10]Liebst, B.S., Garrard, W.L., and Adams, W.M., "Design of an Active Flutter Suppression System," *Journal of Guidance, Control and Dynamics,* Vol. 8, Jan.-Feb. 1986, pp. 64-71.

[11]Moore, B.C., "On the Flexibility Offered by Full State Feedback In Multivariable Systems Beyond Closed Loop Eigenvalue Assignment," *IEEE Transactions on Automatic Control,* Vol. 21, Oct. 1976, pp. 682-691.

[12]Kwakernaak, H. and Sivan, R., *Linear Optimal Control Systems,* Wiley, New York, 1972.

[13]Safanov, M.G. and Athans, M., "Gain and Phase Margins of Multiloop Regulators," *IEEE Transactions on Automatic Control,* Vol. 22, April 1977, pp. 172-179.

[14]Doyle, J.C. and Stein, G., "Multivariable Feedack Design: Concepts for a Classical/Modern Synthesis," *IEEE Transactions on Automatic Control,* Vol. 26, Feb. 1981, pp. 4-16.

[15]Andry, A.N., Shapiro, E.Y., and Chung, J.C., "On Eigenstructure Assignment for Linear Systems," *IEEE Transactions on Aerospace Systems,* AES-19, Sept. 1983, pp. 711-729.

[16]Kazerooni, H., and Houpt, P.K., "On the Loop Transfer Recovery," *International Journal of Control,* Vol. 43, 1986, pp. 981-996.

[17]Lehtomaki, N.A., Sandell, N.R., and Athans, M., "Robustness Results in Linear Quadratic Based Multivariable Controller Design," *IEEE Transactions on Automatic Control,* Vol. 26, Feb. 1981, pp. 75-92.